Conservation of the Conformation of the Porphyrin Macrocycle in Hemoproteins

Walter Jentzen,* Jian-Guo Ma,*# and John A. Shelnutt*#
*Catalysis and Chemical Technologies Department, Sandia National Laboratories, Albuquerque, New Mexico 87185-0710, and #Department of Chemistry, University of New Mexico, Albuquerque, New Mexico 87131 USA

ABSTRACT The out-of-plane distortions of porphyrins in hemoproteins are characterized by displacements along the lowest-frequency out-of-plane normal coordinates of the D_{4h}-symmetric macrocycle. X-ray crystal structures are analyzed using a computational procedure developed for determining these orthogonal displacements. The x-ray crystal structures of the heme groups are described within experimental error, using the set composed of only the lowest frequency normal coordinate of each out-of-plane symmetry type. That is, the distortion is accurately simulated by a linear combination of these orthonormal deformations, which include *sad*dling (B_{2u}), *ruf*fling (B_{1u}), *dom*ing (A_{2u}), *wav*ing (E_g), and *pro*pellering (A_{1u}). For example, orthonormal structural decomposition of the hemes in deoxymyoglobins reveals a predominantly *dom* heme deformation combined with a smaller *wav*(*y*) deformation. Generally, the heme conformation is remarkably similar for proteins from different species. For cytochromes *c*, the conformation is conserved as long as the amino acids between the cysteine linkages to the heme are homologous. Differences occur if this short segment varies in the number or type of residues, suggesting that this small segment causes the nonplanar distortion. Some noncovalently linked hemes like those in the peroxidases also have highly conserved characteristic distortions. Conservation occurs even for some proteins with a large natural variation in the amino acid sequence.

INTRODUCTION

The possible biological significance of nonplanar porphyrin structures in proteins has been suggested by several authors (Kratky et al., 1982; Waditschatka et al., 1985; Geno and Halpern, 1987; Furenlid et al., 1990). For example, a large nonplanar distortion of the heme is observed in the crystal structures of the mitochondrial cytochromes *c* (Berghuis and Brayer, 1992), and this distortion is generally conserved in proteins isolated from different species (Hobbs and Shelnutt, 1995). The importance of these nonplanar heme structures is underscored by the observation that the heme is nonplanar only if the surrounding protein exerts the necessary external forces on the prosthetic group. In contrast, the isolated heme group in solution is planar (Anderson et al., 1993). Thus it is reasonable to suggest that nonplanar porphyrins (Shelnutt et al., 1998) and protein-induced changes in the nonplanarity may provide a mechanism for protein modulation of biological properties.

In a previous paper (Jentzen et al., 1995), a framework for classifying the porphyrin distortions in terms of equivalent displacements along the lowest-frequency normal coordinates of the porphyrin macrocycle was briefly described. We have now extended and refined this idea by developing a computational procedure for determining (for any porphyrin structure) the out-of-plane and in-plane displacements along all of the normal coordinates of the macrocycle (Jentzen et al., 1997). This method has now been used successfully to analyze the macrocyclic distortions in crystal structures of more than 400 hemoproteins and synthetic metalloporphyrins. As expected on physical grounds, only the lowest frequency normal coordinates of each symmetry type (minimal basis set) are needed to adequately simulate the macrocyclic distortions that are observed in the x-ray crystal structures of the hemoproteins. Consequently, displacements along only the six lowest frequency out-of-plane normal coordinates are necessary to uniquely characterize the heme distortions observed in the x-ray crystal structures of the hemoproteins. The complexity of the heme distortions and the lack of a simple way of characterizing them previously hid several possible relationships between protein function and heme distortion. Unfortunately, the same analysis of the relatively small in-plane displacements is not as successful, because they are near the estimated positional uncertainties for hemoproteins (Jentzen et al., 1997).

In this work we first describe a short version of the full normal-coordinate structural decomposition (NSD) method that uses only the six lowest frequency out-of-plane normal coordinates of the macrocycle. The complete description, including all normal modes of the D_{4h}-symmetric macrocycle (complete basis), is given elsewhere (Jentzen et al., 1997). The NSD procedure is then used to determine the amounts of the saddling (*sad*, B_{2u}), ruffling (*ruf*, B_{1u}), doming (*dom*, A_{2u}), waving [*wav*(*x*), *wav*(*y*); E_g], and propellering (*pro*, A_{1u}) deformation types required to simulate the observed out-of-plane distortion of the heme macrocycle(s) for each protein. For example, the heme from sperm whale deoxymyoglobin is found by the NSD procedure to be mainly domed with a minor contribution from the *wav*(*y*) deformation. More importantly, the heme conforma-

Received for publication 3 July 1997 and in final form 23 October 1997.
Address reprint requests to Dr. John A. Shelnutt or Dr. Walter Jentzen, Catalysis and Chemical Technologies Department, Sandia National Laboratories, Albuquerque, NM 87185-0710. Tel.: 505-272-7160; Fax: 505-272-7077; E-mail: jasheln@unm.edu.

0006-3495/98/02/753/11 $2.00

tion is found to be a distinguishing characteristic of some classes of proteins. Specifically, the heme conformations of several different types of hemoprotein (peroxidase, cytochrome P450, cytochrome *c*, cytochrome *c′*, and cytochrome c_3) are conserved. In addition, for the *c*-type cytochromes, the role of the short covalently linked protein segment (Cys-X-Y-Cys-His) in causing the heme distortion is clarified by comparison of the decomposition results for several types of cytochromes. Two general conclusions emerge from this analysis. First, there are large differences in heme distortions in both type and magnitude of the contributing normal deformations. Second, for proteins belonging to a single functional class, strong similarities in the heme conformation are found.

METHODS

A minimal normal-mode basis for the description of nonplanar heme distortions

The description of the nonplanar porphyrin distortion in terms of equivalent displacements along the out-of-plane normal coordinates of the macrocycle provides a uniquely useful framework for analyzing the porphyrin structure. The lowest frequency normal coordinates of each symmetry type are the softest modes of distortion, i.e., the restoring forces (or distortion energies) are the smallest for displacements along these coordinates. Thus these deformations are expected to predominate in the observed heme distortion. Furthermore, because the out-of-plane displacements along these normal coordinates are the largest, they are the most statistically significant. In addition, expressing the distortion in terms of only the six (out-of-plane) normal deformations [*sad* (B_{2u}), *ruf* (B_{1u}), *dom* (A_{2u}), *wav*(*x*), *wav*(*y*) (E_g), *pro* (A_{1u})] greatly simplifies the description of the heme conformation. That is, static (1-Å) deformations along the lowest frequency out-of-plane normal modes of each symmetry type form a minimal basis for representing the distortions. In fact, only five values must be given to characterize the structure, because the *pro* deformation is usually too small to be statistically significant (vide infra). For these reasons, only a simplified version of the full procedure for normal structural decomposition in terms of all of the normal modes (Jentzen et al., 1997) is described and utilized here for analysis of the hemoprotein crystal structures.

Linear combinations of the minimal-basis normal-coordinate deformations

Fig. 1 illustrates static 1-Å deformations along the lowest frequency normal mode of each symmetry type. The atomic displacements shown and the frequencies given in Fig. 1 are for the normal modes of the D_{4h}-symmetric copper macrocycle that is our reference structure. A complete discussion of this choice for the reference structure is given elsewhere (Jentzen et al., 1997). Briefly, the energy-minimized reference structure and normal modes are obtained by using a molecular mechanics force field developed for metalloporphyrins (Shelnutt et al., 1991; Song et al., 1996). The 1-Å normalized static displacements shown in Fig. 1 are defined in non-mass-weighted coordinate space and are referred to as normal deformations. An observed structure is analyzed by projecting out the displacement along these normal deformations [B_{2u} (*sad*, 65 cm^{-1}), B_{1u} (*ruf*, 88 cm^{-1}), A_{2u} (*dom*, 135 cm^{-1}), E_g [*wav*(*x*), *wav*(*y*); 176 cm^{-1}], and A_{1u} (*pro*, 335 cm^{-1})] (Jentzen et al., 1997). Then a simulated heme structure is obtained by forming the linear combination of normal deformations determined by these displacements, and the simulated and observed structures are compared in a linear display (see Figs. 3 and 5).

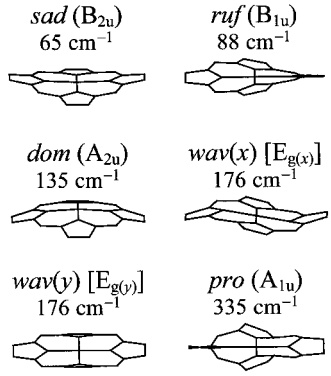

FIGURE 1 Illustrations of the lowest-frequency out-of-plane eigenvectors in the coordinate space, for each of the normal deformations $\hat{\mathbf{D}}_k$ (*k*: *sad, ruf, dom, wav*(*x*), *wav*(*y*) and *pro*) used in describing the nonplanar distortions of the porphyrin macrocycle. Static displacements representing a 1-Å deformation along each lowest frequency normal coordinate are shown, i.e., the square root of the sum of the squares of the displacements of the 24 atoms of the macrocycle is 1 Å.

Mathematically, the nonplanar heme distortion is simulated by a particular linear combination of the six normal deformations according to

$$\Delta\mathbf{z}_{sim} = d_{sad}\hat{\mathbf{D}}_{sad} + d_{ruf}\hat{\mathbf{D}}_{ruf} + d_{dom}\hat{\mathbf{D}}_{dom} + d_{wav(x)}\hat{\mathbf{D}}_{wav(x)} + d_{wav(y)}\hat{\mathbf{D}}_{wav(y)} + d_{pro}\hat{\mathbf{D}}_{pro} = \sum_{k=1}^{6} d_k\hat{\mathbf{D}}_k \quad (1)$$

where $\Delta\mathbf{z}_{sim}$ is the 24-dimensional vector of displacements for the macrocyclic atoms from the mean plane for the simulated structure. (The method for calculating a (least-squares) mean plane to a set of points has been given by Schomaker and co-workers (Schomaker et al., 1959). The points can be either the x-ray atomic coordinates of the observed structure or the coordinates of the simulated structure.) The normalized vectors $\hat{\mathbf{D}}_k$ are the 24-dimensional basis vectors (normal deformations) shown in Fig. 1 (Jentzen et al., 1997); the subscript *k* designates the *sad, ruf, dom, wav*(*x*), *wav*(*y*), and *pro* normal-deformation types. The scalar coefficients d_k (in Å) are the displacements along the normal deformations $\hat{\mathbf{D}}_k$.

Determination of the displacements along the normal deformations

The displacements d_k in Eq. 1 are obtained by the least-squares method. That is, the d_k are determined by requiring that the sum of the least-squares residuals between the simulated, $\Delta\mathbf{z}_{sim}$, and observed, $\Delta\mathbf{z}_{obs}$, distortions is a minimum,

$$f(d_k) = |\Delta\mathbf{z}_{sim} - \Delta\mathbf{z}_{obs}|^2 = \left|\sum_{k=1}^{6} d_k\hat{\mathbf{D}}_k - \Delta\mathbf{z}_{obs}\right|^2 \overset{!}{=} \text{minimum} \quad (2)$$

where the vertical bars represent the norm of the vector. Equation 2 requires six equations:

$$\frac{\partial f(d_k)}{\partial d_k} = 0, \quad (3)$$

where *k*: *sad, ruf, dom, wav*(*x*), *wav*(*y*) and *pro*

Because the normal deformations are orthogonal by symmetry ($\hat{\mathbf{D}}_k'\hat{\mathbf{D}}_j = \delta_{kj}$), the solution is then simply

$$d_k = \hat{\mathbf{D}}_k' \, \Delta\mathbf{z}_{obs} \tag{4}$$

This set of displacements d_k determines the total simulated distortion D_{sim}^{oop} (in Å). Using Eq. 1, we then obtain

$$D_{sim}^{oop} = |\Delta\mathbf{z}_{sim}(d_k)| = \sqrt{\sum_{k=1}^{6} d_k^2} \tag{5}$$

The total observed distortion D_{obs}^{oop} is given by the observed atomic Δz displacements of each of the 24 macrocyclic atoms $(\Delta z_n)_{obs}$ with respect to the mean plane:

$$D_{obs} = \sqrt{\sum_{n=1}^{24} (\Delta z_n)_{obs}^2} = |\Delta\mathbf{z}_{obs}| \tag{6}$$

Estimation of the goodness of the simulated structures

Because we are using a truncated basis set, the minimal basis does not give exact agreement between the observed and simulated distortion. A measure of the goodness of the simulated distortion is required. In x-ray protein crystallography, the mean positional error for a single atom is commonly used to estimate the error in the atomic positions (Luzzati, 1952; Matsuura et al., 1982). (Sometimes the root-mean-square (rms) deviation is also given for the error estimate in the x-ray crystallography. Assuming a normal probability density function for the deviations (or positional errors), it can be shown that the mean deviation in one dimension is lower than the rms deviation by a factor of $\sqrt{2/\pi}$ (Jentzen and Shelnutt, unpublished results). Hence the mean and rms deviations are almost identical, and each serves as an error estimate for the atomic positions.) In our case, the mean deviation $\bar{\delta}_{oop}$ between the simulated and observed out-of-plane displacements, given by

$$\bar{\delta}_{oop} = \frac{1}{24} \sum_{n=1}^{24} |(\Delta z_{sim})_n - (\Delta z_{obs})_n| \tag{7}$$

is a useful quantity that is related to the mean positional uncertainty. In this equation, the vertical bars represent the absolute value of a scalar quantity.

According to the Luzzati method for analyzing the error in the x-ray structure, the mean positional error for a single atom is ~0.10–0.20 Å at ~2.0-Å resolution (Matsuura et al., 1982). Because of the underlying assumption in the Luzzati treatment, this value is known to be an upper limit of the true coordinate errors. On the other hand, the mean positional error from the diagonal of the least-squares normal matrix (Cruickshank, 1960) gives a lower limit; this value is typically ~0.06 Å (Matsuura et al., 1982). However, in our case, the lower- and upper-limit mean errors in the atomic positions (Δz displacement) are estimated to be lower by a factor of 0.5 because of the dimensionality (Jentzen and Shelnutt, unpublished results). Accordingly, the lower and upper limits of the mean positional error in one dimension are estimated to be ~0.03 and 0.10 Å, respectively. These statistical errors in the x-ray structure serve as a reference when considering the goodness of fit for the simulated conformation. Thus we conclude that the minimal basis is sufficient for simulating the heme distortion if the mean deviation $\bar{\delta}_{oop}$ is lower than or equal to 0.03 Å.

Estimation of the macrocycle distortion energy

For small displacements (harmonic approximation), the total macrocyclic distortion energy is simply the sum of energy terms for each of the out-of-plane normal-mode coordinates. In terms of the displacements d_k, the total distortion energy is estimated from

$$V_{oop} = \sum_{k=1}^{6} V_{oop}(d_k) = 2\pi^2 c^2 \sum_{k=1}^{6} \tilde{\nu}_k^2 \mathbf{Q}_k^2 = \sum_{k=1}^{6} K_k d_k^2 \tag{8}$$

$\mathbf{Q}_k$ is the root-mass-weighted normal coordinate, $\tilde{\nu}_k$ (in cm^{-1}) is the vibrational frequency of the kth mode, and c is the speed of light. The force constant, K_k (in kJ mol^{-1} $Å^{-2}$), is associated with the distortion energy for a 1-Å displacement in the non-mass-weighted coordinate system. The force constant depends on the square of the vibrational frequency and, to a lesser extent, on the atomic masses. Using the molecular mechanics frequencies for the copper-macrocycle reference structure, these energies for the 1-Å deformation are 9.1 (*sad*), 16.5 (*ruf*), 41.3 (*dom*), 67.3 (*wav*), and 238.4 kJ mol^{-1} (*pro*) (Jentzen et al., 1997).

It is important to remember that the frequencies used for determining the deformational energies are for the normal modes of the "bare" macrocycle. That is, the frequencies are for the carbons and nitrogens of the porphyrin skeleton, with the hydrogen and metal masses set to zero. These are not the normal modes of a specific substituted porphyrin, like NiOEP. For example, the mode γ_9 of NiOEP is composed of the doming mode of the macrocycle mixed with in-phase A_{2u} motions of the ethyl substituents. It is, in fact, mostly a substituent mode. The substituent motions lower the frequency of the doming mode of the macrocycle with which it is mixed to 32 cm^{-1} for NiOEP. By using the modes of the macrocycle and not a specific substituted porphyrin, the method is much more general, and we obtain estimates of the deformational energy of just the macrocycle. In general, the doming contribution obtained from the NSD analysis is distributed among several A_{2u} normal modes for a specific substituted porphyrin. The energetic estimates for the *dom* deformation obtained from NSD will include the contributions for all of the normal modes of a substituted porphyrin that include *dom* mode contributions. Because it is the deformational energies of the macrocycle that are of interest, the macrocyclic normal modes are the correct choice for our structural analysis, not those of a particular substituted porphyrin.

From the energies of deformation, K_k, the perturbation energy causing the macrocyclic distortion (e.g., steric interaction energy of bulky substituents) is most easily channeled into the *sad* and *ruf* deformations, less easily into the *dom* and *wav* deformations, and almost never into the *pro* deformation. The actual deformations observed depend not only on the energy, however, but also on how efficiently a particular normal deformation relieves the perturbing interaction. This is seen most clearly in the x-ray crystal structures of symmetrical tetrasubstituted porphyrins, for which a nearly pure out-of-plane displacement along only one of the lowest-frequency normal coordinates is commonly observed (Jentzen et al., 1995, 1997). Pure displacements along one of the lowest-frequency normal coordinates give the frequently observed ruffled (*ruf*, B_{1u}), saddled (*sad*, B_{2u}), and domed (*dom*, A_{2u}) distortions, similar to those illustrated in Fig. 1 (Jentzen et al., 1997). Significant distortions along the *wav* and *pro* coordinates are rarely seen, because the energy required to induce a distortion along a particular normal coordinate goes up as the square of the frequency of the mode. Thus the distortion energy, in this case provided by the steric repulsion of the peripheral substituents, is apparently too small to induce significant distortions along these higher frequency normal coordinates. In particular, this explains why the lowest-frequency A_{1u} normal coordinate at 335 cm^{-1} (twisting of the pyrrole rings as in a propeller) is not required in the sum of Eq. 1. That is, the *pro* mode is too high in frequency and thus usually requires too much energy to contribute significantly to the observed distortion. Viewed in another way, caution should be exercised in drawing conclusions from this estimate of the distortion energy, because even small deformations for high-frequency modes are energetically significant.

Whereas using only the minimal basis in the normal-coordinate structural decomposition is successful for describing the nonplanar heme distortions for the proteins, the simulated and observed structures significantly deviate for the high-resolution x-ray crystal structures of synthetic metalloporphyrins (Jentzen et al., 1997). In this case, an essentially exact

simulation is obtained for the out-of-plane distortion by using a basis set of deformations expanded to include the second lowest-frequency mode of each symmetry type (extended basis set). The high resolution of x-ray structures of the synthetic porphyrins allows the small contributions of the higher frequency normal deformations to be observed. A discussion of the mathematical procedure for normal-coordinate structural decomposition using all of the normal coordinates, a discussion of the limits of using the minimal basis set of normal coordinates, and application to the analysis of synthetic porphyrin crystal structures and additional protein-bound porphyrin structures are given elsewhere (Jentzen et al., 1997).

RESULTS AND DISCUSSION

Normal-coordinate structural decomposition

The description of a porphyrin structure in terms of the normal coordinates is a uniquely useful way of characterizing the macrocyclic structure. Unlike other descriptions, the normal-coordinate-structural-decomposition method occupies a special status because of the unique relationship between the macrocyclic distortion energies and the displacements along the normal coordinates. In other words, if the displacement d_k for each normal-coordinate deformation is known, then the total macrocyclic-distortion energy can be readily estimated by using Eq. 8. Furthermore, a great simplification occurs when the porphyrin distortion is expressed in terms of normal coordinates. The simplification results from the fact that only a few (five or six) displacements, i.e., the d_k for the lowest frequency modes of the macrocycle, must be specified to fully characterize the distortion. The mean deviation $\bar{\delta}_{oop}$ between the simulated and observed out-of-plane displacements is, in most cases, not significantly higher than the minimum experimental error of $\sim$0.03 Å. In fact, the mean deviation for the proteins analyzed in this work is, on average, 0.028 Å, with a standard deviation of 0.014 Å. This value is similar to the expected mean (one-dimensional) positional errors in the x-ray protein structures.

Previously used structural parameters for characterizing the observed distortion can be estimated from the magnitude of the normal deformations (Jentzen et al., 1995; Shelnutt et al., 1991, 1992; Medforth et al., 1992; Hobbs et al., 1994). For example, the tilt angle N-M-N and the C_αN-NC_α dihedral angle of opposite pyrrole planes were used to characterize the *sad* and *ruf* deformation types, respectively. We can now examine the ability of these structural parameters to quantify the contributions of the normal deformations to a particular structure. It turns out that these structural parameters are good measures of the displacements along each of these normal deformations, that is, these parameters are proportional to the associated deformations for small displacements (Jentzen et al., 1997). Moreover, given the proportionality constants, the deformations can be calculated from these structural parameters. Thus a 1-Å pure *sad* deformation is equivalent to a 4.2° decrease in the N-M-N pyrrole tilt angle from 180°, and a 1-Å *ruf* deformation is equivalent to an increase in the C_αN-NC_α dihedral angle of $\sim$22° (Jentzen et al., 1997). (For example, the observed ruffling angle C_αN-NC_α of the crystal structure of the tetragonal form of Ni(OEP) is 32.8° (Meyer, 1972; Jentzen et al., 1996). The decomposition method reveals for this porphyrin a pure *ruf* deformation type; the *ruf* displacement is 1.456 Å (Jentzen et al., 1997). Using a linear relationship, the estimated ruffling angle is then 32.0° [= (22.0 deg Å^{-1}) $\times$ (1.456 Å)], a value that is close to that observed.)

Structural decomposition of the hemes in x-ray crystal structures of proteins

The asymmetrical protein environment induces simultaneous displacements along several or all of the lowest frequency normal coordinates, making the nonplanar distortion difficult to characterize by eye. However, normal-coordinate structural decomposition projects these contributions out, providing a sensitive descriptor for these complicated structures. Most importantly, by using the structural decomposition method, we are more likely to discover relationships among the molecular structure, spectroscopic features, and biological function. The latter statement follows from the unique relationship between the normal deformations (d_k) and the vibrational and static distortion energies.

Deoxymyoglobin

The analysis of the heme groups from sperm whale deoxymyoglobin provides an interesting first example. The decomposition results for crystal structures (Yang and Phillips, 1996) of sperm whale myoglobin under various crystallization conditions are illustrated in Fig. 2; the different myoglobin structures are labeled in Fig. 2 with the Brookhaven Protein Data Bank (PDB) (Bernstein et al., 1977; Abola et al., 1987; Stampf et al., 1995) reference codes and the pH of the crystallization. The observed and simulated out-of-plane distortions for one of the deoxyhemes are shown in Fig. 3 *A* in a clothesline linear display. In all, five deoxymyoglobin x-ray crystal structures are known from three independent working groups. The structures from Yang et al. (Yang and Phillips, 1996) are from crystals grown at pH 4.0 (1vxa), 5.0 (1vxd), and 6.0 (1vxg). The myoglobin structures of Takano (Takano, 1984) and Phillips et al. (Phillips and Schoenborn, 1981), which are not shown in Fig. 2, were obtained from crystals at pH 5.8 (5mbn) and pH 8.4 (1mbd), respectively. The five deoxy structures are remarkably similar, based on the standard deviations of the displacements of $\sim$0.1 Å. The deviations are similar to those of the 11 α-hemes and 11 β-hemes of human deoxyhemoglobin A crystal structures (Jentzen et al., 1997).

Because there are functional similarities between the hemes of human hemoglobin (oxygen transport) and the heme of myoglobin (oxygen storage), it was of interest to see whether the structural decomposition method would reveal similarities and differences between the heme distortions. The examination of the displacements for the hemes

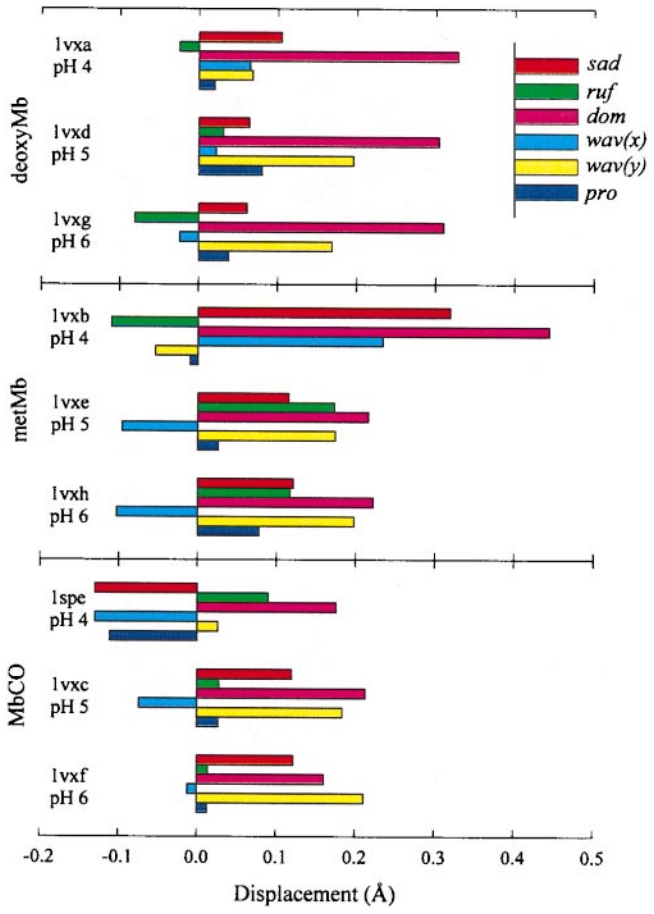

FIGURE 2 Out-of-plane displacements for the heme groups of x-ray crystal structures of deoxymyoglobin, metmyoglobin, and carbonmonoxymyoglobin (Yang and Phillips, 1996; Takano, 1984; Phillips and Schoenborn, 1981). PDB reference codes are also given. In the simulation, the macrocycle is oriented according to Fig. 3 *A*. The x-ray crystal structure resolution and crystallization condition are 1vxa (2.0 Å), pH 4; 1vxd (1.7 Å), pH 5; 1vxg (1.7 Å), pH 6 for the deoxy protein; 1vxb (2.0 Å), pH 4; 1vxe (1.7 Å), pH 5; 1vxh (1.7 Å), pH 6 for metmyoglobin; and 1spe (2.0 Å), pH 4; 1vxc (1.7 Å), pH 5; 1vxf (1.7 Å), pH 6 for carbonmonoxymyoglobin (Yang and Phillips, 1996).

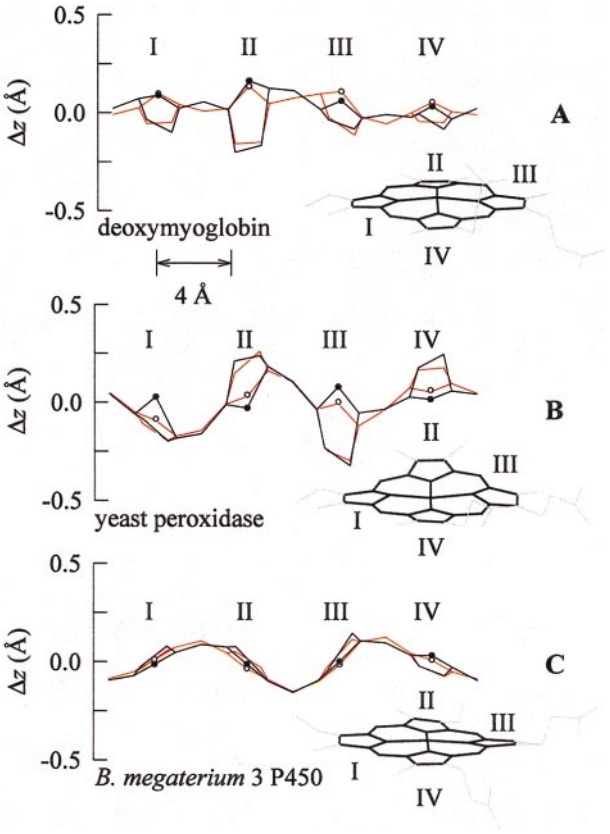

FIGURE 3 X-ray crystal structures of the heme groups of deoxymyoglobin (*A*) (Yang and Phillips, 1996), peroxidase (*B*) (Finzel et al., 1984), and P450 (*C*) (Li and Poulos, 1995). The out-of-plane distortion is illustrated in a clothesline display of the observed (*black lines*) and simulated (*red lines*) displacements of the 24 atoms with respect to the mean plane. The PDB reference code, the location of the axial ligand in the simulation, and the x-ray crystal structure resolution for myoglobin are given in the legend of Fig. 2 (1vxg). Similar information for yeast cytochrome *c* peroxidase and *Bacillus megaterium* cytochome P450 are given in the legend of Fig. 4.

in deoxymyoglobins (Fig. 2) shows that the heme is primarily domed (0.3 Å), and a small but a significant *wav*(*y*) contribution (0.15 Å) is also present. The total heme distortion is 0.4 Å. For comparison, the α-hemes of human deoxyhemoglobin are also primarily domed (0.5 Å), but exhibit a secondary *ruf* deformation (0.3 Å); the β-hemes exhibit almost equal amounts of the *sad* and *dom* deformation types (0.4 Å) (Jentzen et al., 1997). The total distortions for the α- and β-hemes are both 0.6 Å. These deformations indicate a specific asymmetrical interaction between the protein environment and the heme group.

There is little change in the structure of deoxymyoglobin with pH. This is reflected in the limited lateral displacement of the heme in the structures at different pH (Yang and Phillips, 1996). The NSD results show that the pH has a minimal effect on the out-of-plane distortion of the heme as well (Fig. 2). This is not the case for metmyoglobin and carbonmonoxymyoglobin. Yang and Phillips showed that that a lateral displacement of the heme occurs at pH 4, but not at pH 5 and 6 for these myoglobin derivatives. Similarly, the NSD results show a large change in out-of-plane conformation at pH 4. Specifically for metmyoglobin at pH 4, the saddling increases, the ruffling changes sign, the doming increases, and the *x*- and *y*-waving contributions change sign relative to myoglobin at pH 5 and 6. The increase in doming at pH 4 is consistent with the lengthening of the Fe-His[93] bond from 2.15 Å at pH 6 to 2.50 Å at pH 4. Carbonmonoxymyoglobin also shows differences in the out-of-plane conformation at pH 4 compared to the pH 5 and 6 proteins. Specifically at pH 4, the saddling changes sign, ruffling may increase, *x*-waving becomes more negative, and *y*-waving vanishes. Doming remains constant. The lateral shift of the heme group of carbonmonoxymyoglobin at pH 4 is in the direction opposite that of the shift for metmyoglobin. In addition, comparing the three myoglobins at pH 6 shows ligand binding effects on the structure of the macrocycle. For example, the six-coordinate met- and car-

bonmonoxymyoglobins show less doming than five-coordinate deoxymyoglobin.

Temperature-dependent x-ray crystallography of myoglobin gives a picture of the protein as a condensed inner core with semiliquid outer shells. This suggests that the number of conformational substates is less in the vicinity of the heme group. In fact, seven heme-contact residues have very small mobilities for myoglobin (Frauenfelder et al., 1979). These residues, together with the axial ligands and other heme-contact residues, are undoubtedly responsible for maintaining the observed nonplanar structure of the heme. Nevertheless, conformational substates are averaged in the x-ray structures and thus in our analysis of the heme conformation. A different mechanism for maintaining the heme conformation is suggested below for *c*-type cytochromes.

The hemes of hemoglobin and myoglobin are alike in that they all exhibit significant doming and are only moderately nonplanar compared to other hemoproteins. It is also interesting to note that the hemes of hemoglobin are more nonplanar than for myoglobin, indicating additional out-of-plane strain. Moreover, the heme of deoxymyoglobin and the α-hemes of deoxyhemoglobin are alike in that the *dom* deformation dominates. For the β-hemes, the *dom* and *sad* deformations are nearly equal.

Peroxidases and cytochromes P450

Fig. 3 (*B* and *C*) illustrates the heme distortion typical of two other types of noncovalently linked heme proteins. The contribution of each deformation type to the observed conformation is graphically shown in Fig. 4. The decomposition results for three representative proteins of each type point out the similarities and variations in the heme conformations within each group.

The hemes of the peroxidases (Finzel et al., 1984; Sundaramoorthy et al., 1994; Kunishima et al., 1994) exhibit strong saddling (-0.6 to -0.9 Å) and a moderate ruffling (-0.3 to -0.7 Å); other deformations are small and negative (-0.1 to -0.2 Å) or are not significant (see legend of Fig. 4). Clearly, the protein matrix induces large total distortions of the macrocycle (0.7–1.2 Å) for the peroxidases and strongly influences the types of deformation that occur. Indeed, the distortion for the peroxidases is one of the largest observed so far for hemes in proteins, and is unusual for a heme that is not covalently linked (vide infra).

The cytochromes P450 (see legend of Fig. 4) show no more than 30% sequence homology, yet the hemes of cytochromes P450 (Li and Poulos, 1995; Hasemann et al., 1994; Poulos et al., 1986) are all ruffled by more than 0.3 Å. On the other hand, there is no clear pattern in the small contributions from the other deformation types. The total distortion is 0.4–0.5 Å.

For both peroxidases and cytochromes P450, the deformation types that contribute to the structure of the heme are maintained across the natural variation in the amino acid sequence that occurs for the different species represented. In addition, because none of these proteins has a covalently attached heme, these distortions are caused by only the weak nonbonding interactions (van der Waals, hydrogen bonding, axial ligation) between the heme and the surrounding protein.

Mitochondrial ferricytochromes c

The *c*-type cytochromes all have covalently attached heme groups, and it might be expected that the protein could distort the heme more through these strong linkages. Indeed, the hemes of the *c*-type cytochromes are generally more nonplanar than those bound to the protein only by weaker interactions (Hobbs and Shelnutt, 1995). In fact, the structural decomposition results show some support for the idea that the covalently linked segment of the protein plays a pivotal role in causing the observed distortion.

The mitochondrial cytochromes *c* (Ochi et al., 1983; Bushnell et al., 1990; Takano and Dickerson, 1980) provide an instructive example (see legend of Fig. 4). The hemes exhibit a large *ruf* deformation (0.7–1.0 Å), with minor *sad* (-0.1 to -0.3 Å) and *x*- and *y*-*wav* (0.1–0.2 Å) contributions (Fig. 4). The total observed distortion ranges from 0.8 to 1.1 Å. (The heme of rice cytochrome *c* is illustrated in Fig. 5 *A*.) The *wav*(*x*) and *wav*(*y*) contributions are small, but they have the effect of making the *meso*-carbon located between pyrroles I and II the farthest atom from the mean plane (Song et al., 1996; Jentzen et al., 1997). The conservation of this structural feature of the hemes of cytochromes *c* has been noted (Hobbs and Shelnutt, 1995; Jentzen et al., 1997). Because pyrroles I and II also bear the covalent attachment points for the protein, this suggests that the peptide segment between and including the cysteine residues (linking the protein to the heme) is instrumental in generating the nonplanar distortion. This view is supported by the fact that a significant difference in structure among the cytochromes *c* exists for yeast isozyme 2. Isoenzyme 2 is the only mitochondrial cytochrome available for which a nonconservative sequence difference occurs in the two residues between the cysteines. (The amino acid residues between the covalently bonded cysteines are for isozyme-1 Ala-Gln and for isozyme-2 Gln-Gln. For isozyme 2 (1yea), the total observed and simulated distortions are 0.732 and 0.698, respectively. The main contributions are the *ruf* (0.480 Å) and almost equal amounts of *wav*(*x*) (0.316 Å) and *wav*(*y*) (0.380 Å) deformation types. The *sad* (0.061 Å), *dom* (0.064 Å), and *pro* (-0.063 Å) deformations are statistically insignificant.) The strong similarity in the structural decomposition results for the other *c*-type cytochromes, some of which are shown in Fig. 4, also supports the assertion of the importance of this segment.

The oxidized cytochromes *c* might have been expected to be more distorted than the reduced proteins because of the slight preference of low-spin Fe(III) for short metal-nitrogen bonds (Hoard, 1973; Scheidt and Reed, 1981). The slightly smaller Fe(III) (1.986 Å) relative to Fe(II) (1.997 Å) (Scheidt and Gouterman, 1983) favors *ruf* or *sad* distortions because these deformations contract the porphyrin core (Song et al., 1996). However, structural decompositions of

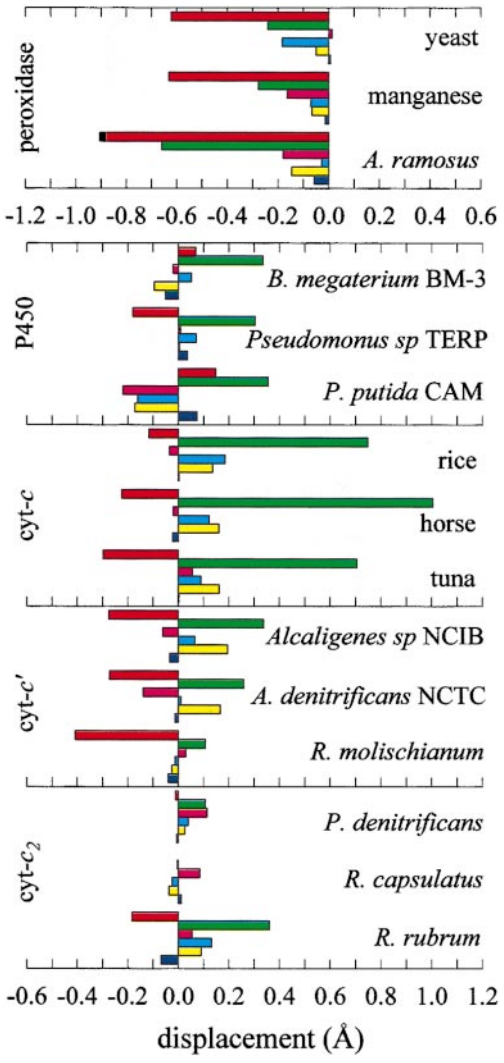

FIGURE 4 Out-of-plane displacements for the heme groups of selected hemoproteins x-ray crystal structures. Color codes are the same as in Fig. 2. For the peroxidases, the macrocycles are oriented as shown in Fig. 3 *B*. Axially ligated histidine is located below the mean plane. The PDB reference code and the x-ray crystal structure resolution for each protein are Baker's yeast (*Saccharomyces cerevisiae*) cytochrome *c* peroxidase (2cyp), 1.7 Å (Finzel et al., 1984); manganese peroxidase from *Phanerochaete chrysosporium* (1mnp), 2.1 Å (Sundaramoorthy et al., 1994); *Arthromyces ramosus* peroxidase (1arp), 1.9 Å (Kunishima et al., 1994). In all peroxidases, a water molecule is localized on the distal side of the heme. For the cytochromes P450, the macrocycle is oriented with its peripheral substituents as shown in Fig. 3 *C*. The axial sulfur ligand is located above the mean plane. The resolution of the x-ray crystal structures and PDB reference codes are *Bacillus megaterium*-3 P450 (2bmh) (dimer of two identical chains A and B; chain A is shown in Fig. 3 *C*), 2.0 Å (Li and Poulos, 1995); *Pseudomonas sp.* TERP P450 (1cpt), 2.3 Å (Hasemann et al., 1994); *Pseudomonas putida* camphor P450, substrate-free (1phc), 1.6 Å (Poulos et al., 1986). A water molecule is an axial ligand to the heme iron in all structures. For the cytochromes *c*, the macrocycle is oriented as shown in Fig. 5 *A*. The axial histidine is located below the mean plane. The amino acid residues between the covalently bonded cysteines are Ala and Gln. The resolution of the x-ray crystal structures and PDB reference codes are rice embryo cytochrome *c* (1ccr), 1.5 Å (Ochi et al., 1983); horse (*Equus caballus*) heart cytochrome *c* (1hrc), 1.9 Å (Bushnell et al., 1990); albacore tuna (*Thunnus alalunga*) heart cytochrome *c* (3cyt), 1.8 Å (Takano and Dickerson, 1980). Cytochrome *c* is a dimer of two identical chains, O (outer molecule) and I (inner molecule). In Fig. 5 *A*, the clothesline display of the heme group for the outer molecule is shown. The cytochromes *c′* were oriented with the macrocycle peripheral substituents as shown in Fig. 5 *B*. Axially ligated histidine is located below the mean plane. The amino acid residues between the covalently bonded cysteines are Lys and Ala. The resolution of the x-ray crystal structures and PDB reference codes are *Alcaligenes sp.*, strain NCIB 11015 cytochrome *c′* (1cgo), 1.8 Å (Dobbs et al., 1996); *Alcaligenes denitrificans*, strain NCTC 8582, cytochrome *c′* (1cgn), 2.2 Å (Dobbs et al., 1996); *Rhodospirillum molischianum* cytochrome *c′* (2ccy), 1.7 Å (Finzel et al., 1985). Cytochrome *c′* is a dimer of two identical chains, A and B. In Fig. 5 *B*, the clothesline display of the heme group in chain A is shown. For the cytochromes c_2, the macrocycle was oriented with its peripheral substituents as shown in Fig. 5 *C*. Axially ligated histidine is located below the mean plane. The resolution of the x-ray crystal structures, the amino acid residues between the covalently bonded cysteines, and PDB reference codes are *Paracoccus denitrificans* cytochrome c_2 (1cot), 1.7 Å, Lys-Ala (Benning et al., 1994); *Rhodobacter capsulatus* cytochrome c_2 (1c2r), 2.5 Å, Lys-Thr (Benning et al., 1991). Cytochrome c_2 is a dimer of two identical chains, A and B. In Fig. 5 *C*, the clothesline display of the heme group in chain A is shown. *Rhodospirillum rubrum* cytochrome c_2 (3c2c), 1.7 Å, Leu-Ala (Bhatia, 1981).

the reduced proteins show no clear consequence of the Fe oxidation state change. For yeast isozyme-1 cytochrome *c* (Berghuis and Brayer, 1992; Louie and Brayer, 1990), the oxidized form is more distorted, but for tuna cytochrome *c* (Takano, 1984; Takano and Dickerson, 1980) there is no clear connection between oxidation state and total distortion. In fact, comparing 10 crystal structures of wild-type mitochondrial cytochromes in ferro and ferri forms shows no clear differences (Jentzen and Shelnutt, unpublished results). In particular, the conserved contributions from strong ruffling and moderate *x*- and *y*-waving exhibit no consistent oxidation-state-dependent differences. It is possible, however, that a larger group of structures or other types of heme proteins will show oxidation-state-specific structural differences. Systematic oxidation-state changes are found in the in-plane structure of the heme in the resonance Raman spectra (Kubitscheck et al., 1986), but these are likely to be far too small to show up in the crystal structures of the proteins.

Ferricytochromes c′

The distortion of one of the *Alcaligenes* cytochromes *c′* is illustrated in Fig. 5 *B*. The hemes of ferricytochromes *c′* (Dobbs et al., 1996; Finzel et al., 1985), like the mitochondrial cytochromes, show a conserved distortion. The total observed distortions are ~0.5 Å. However, as can be seen from Fig. 4, their structures are markedly different from those of the mitochondrial cytochromes *c*. The conservation is understandable for the *Alcaligenes* strains, because the sequence homology is greater than 90% (Dobbs et al., 1996). However, because the sequence identity is only ~30% for the *Alcaligenes* strains and *Rhodospirillum molischianum*, significant heme conformational differences between these proteins are observed. Nonetheless, they all possess mainly *sad* (−0.3 to −0.4 Å) and *ruf* (0.1 to 0.3 Å) deformations, unlike the mitochondrial cytochromes, which are primarily ruffled.

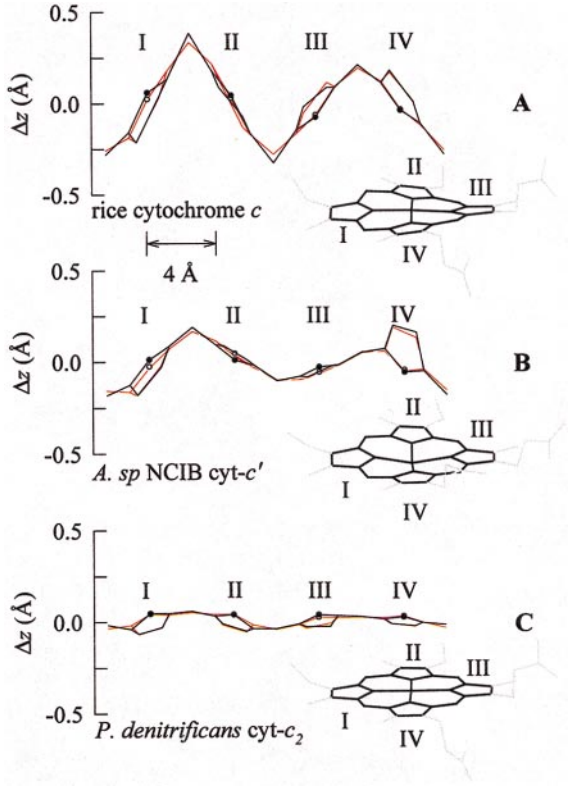

FIGURE 5 X-ray crystal structures of the heme groups of cytochrome *c* (*A*) (Ochi et al., 1983), cytochrome *c′* (*B*) (Dobbs et al., 1996), and cytochrome c_2 (*C*) (Benning et al., 1994). The out-of-plane distortion is illustrated by a linear display of the observed (*black lines*) and simulated (*red lines*) displacements of the 24 atoms with respect to the mean plane. The PDB reference code, the location of the axial ligand in the simulation, and the x-ray crystal structure resolution for each protein are given in the legend of Fig. 4.

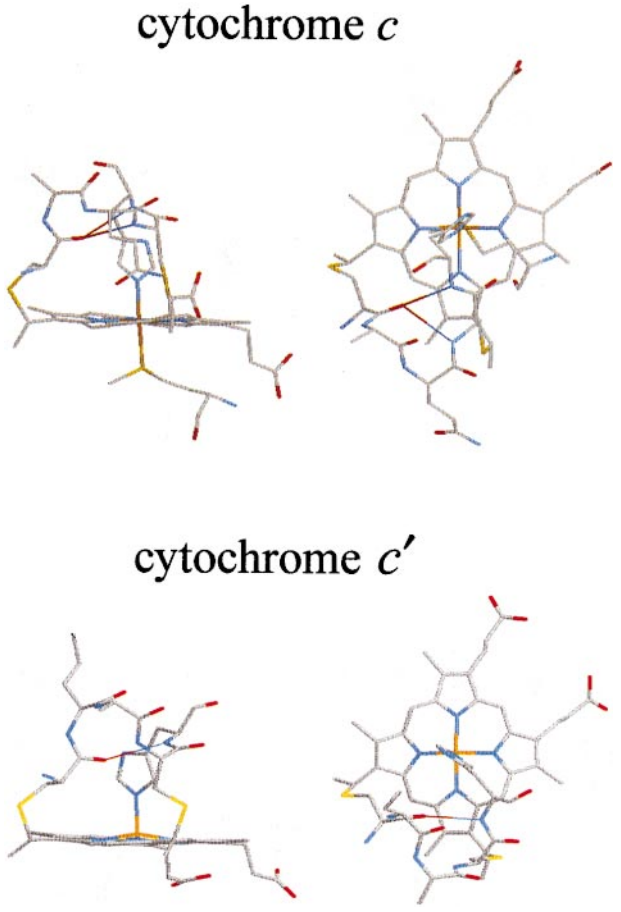

FIGURE 6 Edge-on and top views of the covalently linked peptide segment of the heme group of cytochrome *c* (rice embryos; Ochi et al., 1983) and cytochrome *c′* (*Alcaligenes sp.*; Dobbs et al., 1996). The peptide segments are Cys-Ala-Gln-Cys-His and Cys-Lys-Ala-Cys-His, respectively. The hydrogen-bonding interactions in the backbone are indicated by solid lines. Figures were created with the molecular visualization program RasMol (Sayle and Milner-White, 1995). The PDB reference code and the x-ray crystal structure resolution for each protein are given in the legend of Fig. 4.

In light of the differences in heme conformations for cytochromes *c* and *c′*, it is interesting to examine the short, covalently linked peptide segment to see how it differs for the two, and, in addition, to see whether these differences are conserved for the two types of proteins. Fig. 6 compares the conformation of this protein segment from the x-ray crystal structures for one of the proteins from each group. Of particular interest is the difference in the number of hydrogen bonds within the peptide backbone. This difference in hydrogen bonding in the peptide segment could easily cause the differences in heme conformation by altering the forces on pyrroles I and II. The differences in the orientation of the histidine ligand could also contribute to the differences in heme conformation for cytochrome *c* and *c′*.

Ferrocytochromes c_2

The *Paracoccus denitrificans* cytochrome c_2 (Benning et al., 1991, 1994; Bhatia, 1981) distortion is illustrated in Fig. 5 *C* (also see legend of Fig. 4). This is the one protein among those analyzed so far in which the heme distortion is not clearly conserved (Fig. 4). These are also among the most planar of the hemes in hemoproteins. The magnitude of nonplanar distortion varies from virtually planar (0.1 Å) to moderately distorted (0.5 Å). Thus the heme is nearly planar but appears to be poised to distort. That is, certain amino acid sequence differences can shift the scales in favor of a more nonplanar conformation. In fact, all of the proteins have significant differences in the two amino acids between the cysteine linkages (Lys-Ala, Lys-Thr, Leu-Ala), but apparently only the Lys/Leu difference in the first residue seems to cause a significant distortion (for *R. rubrum*).

Cytochromes c_3

Another interesting example is the four-heme cytochromes c_3 (Morimoto et al., 1991; Higuchi et al., 1984; Morais et al., 1995; Czjzek et al., 1994, 1996), for which the four hemes in the proteins vary remarkably in their structure. Here, too, the differences in structure can be associated with

variations in the peptide segments linking the hemes to the protein (Jentzen et al., 1997). Fig. 7 shows the structural decomposition results for each of the four hemes for cytochromes c_3 from six different strains. (The total observed distortions are, on average, 0.83(5), 0.98(16), and 0.51(15) Å for all hemes 1, hemes 2, and hemes 3 (the values in parentheses are the standard deviations). The overall distortion for hemes 4, excluding the *D. baculatum* strains, is 1.17(8) Å. Finally, the total observed distortions for hemes 4 from the *D. baculatum* strains are 0.8 and 0.4 Å, respectively. The heme numbering scheme is based on the appearance of the heme-binding cysteine residues in the primary sequence, e.g., heme 1 has the lowest numbered cysteines.) Hemes 1 through 3 maintain similar conformations in the proteins from the strains of *Desulfovibrio vulgaris* (Morimoto et al., 1991; Higuchi et al., 1984), *D. desulfuricans* (Morais et al., 1995), *D. gigas* (Matias et al., 1996), and *Desulfomicrobium baculatum* (Czjzek et al., 1994, 1996), and this conservation is surprising, because only a few residues—other than the eight axial histidines and eight cysteines covalently bound to the heme—are conserved. Heme 4 is the exception to the conservation of heme conformation. Hemes 4 have different distortions for the *Desulfomicrobium baculatum* strains than for the others. Examination of the amino acid sequences for the proteins reveals that these strains have a deletion of two of the four residues that are present between the cysteines for heme 4 of the other cytochromes c_3 (Table 1). This clearly points to the pivotal role of this short protein segment. Furthermore, hemes 1 and 3, like hemes 4 of the strains of *D. baculatum*, the mitochondrial cytochromes *c*, and the cytochromes *c′*, have only two residues between the cysteine linkages, and all exhibit a positive *ruf* deformation. This observation again indicates the importance of this heme-linked protein segment. In contrast, hemes 2 and 4, excluding the strains from *D. baculatum*, all have four residues between the cysteines, and, in this case, the main distortion type can be either a *ruf* or a *sad* deformation. Thus not only the number of residues between the cysteines is important, but also the types of residues and the multitude of interactions between

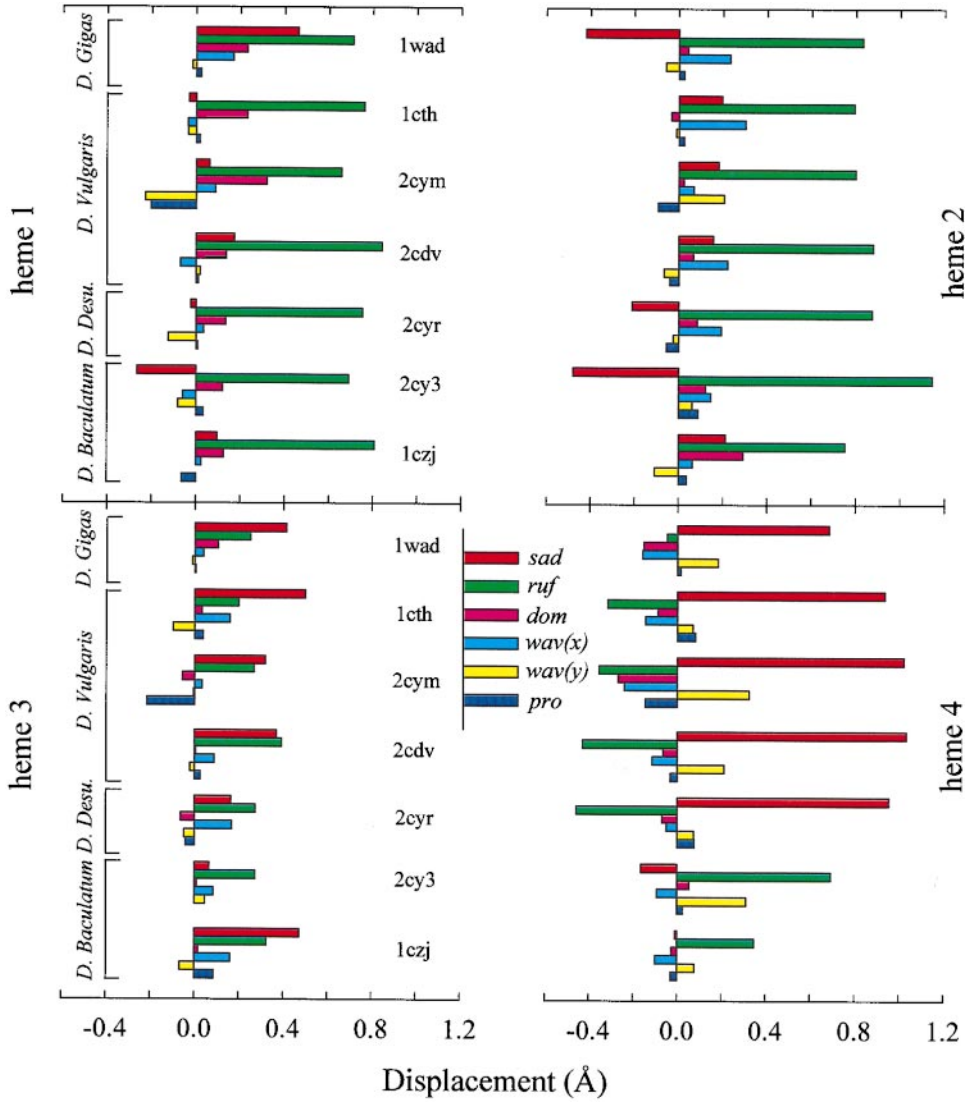

FIGURE 7 Out-of-plane displacements (minimal basis) for the four heme groups in the x-ray crystal structures of cytochromes c_3 from *D. vulgaris* [Hildenborough (Morimoto et al., 1991) and Miyazaki (Higuchi et al., 1984)], *D. desulfuricans* [ATCC 27774 (Morais et al., 1995)], D. gigas (Matias et al., 1996), and two strains from *Desulfomicrobium baculatum* [Norway 4 (Czjzek et al., 1994) and Norway NCIB 8310 (Czjzek et al., 1996)]. For the cytochromes c_3, the displacements were obtained by orienting the macrocycle with its peripheral substituents as shown in Fig. 5. The PDB reference codes and the x-ray crystal structure resolutions are *Desulfovibrio vulgaris*, strain Hildenborough (2cym), 2.0 Å (Morimoto et al., 1991); *Desulfovibrio vulgaris*, strain Miyazaki (2cdv), 1.8 Å (Higuchi et al., 1984): *Desulfovibrio desulfuricans*, strain ATCC 27774 (2cyr), 1.8 Å (Morais et al., 1995); *Desulfomicrobium baculatum*, strain Norway 4, (2cy3) 1.7 Å (Czjzek et al., 1994) and strain Norway NCIB 8310 (1czj), 2.2 Å, (Czjzek et al., 1996); and *Desulfovibrio gigas* (1wad), 1.8 Å (Matias et al., 1996).

TABLE 1 Covalently linked peptide segments of the four heme groups in cytochrome c_3 from *Desulfovibrio vulgaris* (Hildenborough and Miyazaki), *D. sulfuricans* (ATCC 27774), *D. gigas,* and *Desulfomicrobium baculatum* (Norway 4 and Norway NCIB 8310)

	D. vulgaris Hildenborough (1cth)	*D. vulgaris* Hildenborough (2cym)	*D. vulgaris* Miyazaki (2cdv)	*D. gigas* (1wad)	*D. desulfuricans* ATCC 27774 (2cyr)	*D. baculatum* Norway 4 (2cy3)	*D. baculatum* NCIB 8310 (1czj)
Heme 1	C**GD**–C	C**GD**–C	C**GD**–C	C**DD**–C	C**VT**–C	C**VQ**–C	C**QQ**–C
Heme 2	C**GTAG**C	C**GTAG**C	C**ATAG**C	C**TTDG**C	C**GSSG**C	C**TTSG**C	C**MTEG**C
Heme 3	C**VG**–C	C**VG**–C	C**VG**–C	C**IS**–C	C**LA**–C	C**ID**–C	C**VG**–C
Heme 4	C**KKSK**C	C**KKSK**C	C**KGSK**C	C**KGSA**C	C**AKSK**C	C-**G-K**C	C**N-S**-C

All of the fifth and sixth axial ligands of the heme iron atoms are histidine nitrogen atoms. One-letter symbols are used for the amino acids (Dayhoff and Eck, 1972).

these residues and with nearby amino acids are similarly important in determining the details of the heme distortion.

CONCLUSIONS

Normal-coordinate structural decomposition furnishes an important new probe of the protein environment of the heme active site that, in some cases, reveals previously hidden influences of the protein on the conformation of the heme. These influences undoubtedly result from the observation that functionally related proteins share the same class of tertiary structures, especially near the functional domains (Lesk and Chotia, 1986a,b; Sweet, 1986; Hasemann et al., 1995). At present, direct relationships between the heme structure and its biological function are still not evident; however, the normal-coordinate structural decomposition method provides the needed framework for systematic exploration of the role of nonplanar distortions of tetrapyrroles in biochemical mechanisms. The method brings to the fore the participation of the low-frequency vibrational modes of the heme and symmetry properties of the protein-heme interaction. In this way, the structural decomposition method potentially facilitates the discovery of correlations between spectral properties and specific types of distortions, and these structural and spectral correlations should aid in the search for relationships between heme structure and function.

We thank Ms. Yan Qiu for help in preparation of the manuscript and figures.

Sandia is a multiprogram laboratory operated by Sandia Corporation, a Lockheed Martin Company, for the U.S. Department of Energy under Contract DE-AC04-94DP85000.

REFERENCES

Abola, E. E., F. C. Bernstein, S. H. Bryant, T. F. Koetzle, and J. Weng. Brookhaven Protein Data Bank. 1987. *In* Crystallographic Databases—Information Content, Software Systems, Scientific Applications. F. H. Allen, G. Bergerhoff, and R. Sievers, editors. Data Commission of the International Union of Crystallography, Bonn, Cambridge, Chester. 107.

Anderson, K. K., J. D. Hobbs, L. Luo, K. D. Stanley, J. M. E. Quirke, and J. A. Shelnutt. 1993. Planar-nonplanar conformational equilibrium in metal derivatives of octaethylporphyrin and *meso*-nitrooctaethylporphyrin. *J. Am. Chem. Soc.* 115:12346–12352.

Benning, M. M., T. E. Meyer, and H. M. Holden. 1994. X-ray structure of the cytochrome c_2 isolated from *Paracoccus denitrificans* refined to 1.7-Å resolution. *Arch. Biochem. Biophys.* 310:460–466.

Benning, M. M., G. Wesenberg, M. S. Caffrey, R. G. Bartsch, T. E. Meyer, M. A. Cusanovich, I. Rayment, and H. M. Holden. 1991. Molecular structure of cytochrome c_2 isolated from *Rhodobacter capsulatus* determined at 2.5-Å resolution. *J. Mol. Biol.* 220:673–685.

Berghuis, A. M., and G. D. Brayer. 1992. Oxidation state-dependent conformational changes in cytochrome *c*. *J. Mol. Biol.* 223:959–970.

Bernstein, F. C., T. F. Koetzle, G. J. B. Williams, E. F. Meyers, M. D. Brice, J. R. Rodgers, O. Kennard, T. Shimanouchi, and M. Tasumi. 1977. The Protein Data Bank: a computer-based archival file for macromolecular structures. *J. Mol. Biol.* 112:535–542.

Bhatia, G. E. 1981. Refinement of the crystal structure of oxidized *Rhodospirillum rubrum* cytochrome c_2. Ph.D. thesis. University of California, San Diego.

Bushnell, G. W., G. V. Louie, and G. D. Brayer. 1990. High-resolution 3-dimensional structure of horse heart cytochrome *c*. *J. Mol. Biol.* 214:585–595.

Cruickshank, D. W. J. 1960. The required precision of intensity measurements for single-crystal analysis. *Acta Crystallogr.* 13:774–777.

Czjzek, M., F. Payan, F. Guerlesquin, M. Bruschi, and R. Haser. 1994. Crystal structure of cytochrome c_3 from *Desulfovibrio desulfuricans* Norway at 1.7-Å resolution. *J. Mol. Biol.* 243:653–667.

Czjzek, M., F. Guerlesquin, M. Bruschi, and R. Haser. 1996. Crystal structure of a dimeric octaheme cytochrome c_3 (M_r 26000) from *Desulfovibrio desulfuricans* Norway. *Structure.* 4:395–404.

Dayhoff, M. O., and R. V. Eck. 1972. Atlas of Protein Sequence and Structures. Biomedical Research Foundation, Washington, DC.

Dobbs, A. J., H. R. Faber, B. F. Anderson, and E. N. Baker. 1996. 3-Dimensional structure of cytochrome *c′* from two Alcaligenes species and the implications for four-helix bundle structures. *Acta Crystallogr. D.* 52:356–368.

Finzel, B. C., T. L. Poulos, and J. Kraut. 1984. Crystal structure of yeast cytochrome *c* peroxidase refined at 1.7-Å resolution. *J. Biol. Chem.* 259:13027–13036.

Finzel, B. C., P. C. Weber, K. D. Hardman, and F. R. Salemme. 1985. Structure of ferricytochrome *c′* from *Rhodospirillum molischianum* at 1.67-Å resolution. *J. Mol. Biol.* 186:627–643.

Frauenfelder, H., G. A. Petsko, and D. Tsernoglou. 1979. Temperature-dependent x-ray diffraction as a probe of protein structural dynamics. *Nature.* 280:558–563.

Furenlid, L. R., M. W. Renner, K. M. Smith, and J. Fajer. 1990. Structural consequences of nickel versus macrocycle reductions in F430 models: EXAFS studies of a Ni(I) anion and Ni(II) π-anion. *J. Am. Chem. Soc.* 112:1634–1635.

Geno, M. K., and J. Halpern. 1987. Why does nature not use the porphyrin ligand in vitamin-B_{12}? *J. Am. Chem. Soc.* 109:1238–1240.

Hasemann, C. A., R. G. Kurumbail, S. S. Boddupalli, J. A. Peterson, J. A. Deisenhofer, and J. Deisenhofer. 1995. Structure and function of cytochromes P450: a comparative analysis of three crystal structures. *Structure.* 3:41–62.

Hasemann, C. A., K. G. Ravichandran, J. A. Peterson, and J. Deisenhofer. 1994. Crystal structure and refinement of cytochrome P450(TERP) at 2.3-Å resolution. *J. Mol. Biol.* 236:1169–1185.

Higuchi, Y., M. Kusunoki, Y. Matsuura, N. Yasuoka, and M. Kakudo. 1984. Refined structure of cytochrome c_3 at 1.8 Å resolution. *J. Mol. Biol.* 172:109–139.

Hoard, J. L. 1973. Some aspects of metalloporphyrin stereochemistry. *Ann. N.Y. Acad. Sci.* 206:18–31.

Hobbs, J. D., S. A. Majumder, L. Luo, G. A. Sickelsmith, J. M. E. Quirke, C. J. Medforth, K. M. Smith, and J. A. Shelnutt. 1994. Structural heterogeneity and coordination chemistry of nickel(II) octaethyl-*meso*-nitroporphyrins. *J. Am. Chem. Soc.* 116:3261–3270.

Hobbs, J. D., and J. A. Shelnutt. 1995. Conserved nonplanar heme distortions in cytochromes *c*. *J. Protein Chem.* 14:19–25.

Jentzen, W., M. C. Simpson, J. D. Hobbs, X.-Z. Song, T. Ema, N. Y. Nelson, C. J. Medforth, K. M. Smith, M. Veyrat, M. Mazzanti, R. Ramasseul, J.-C. Marchon, T. Takeuchi, W. A. Goddard, III, and J. A. Shelnutt. 1995. Ruffling in a series of nickel(II) *meso*-tetrasubstituted porphyrins as a model for the conserved ruffling of the heme of cytochromes *c*. *J. Am. Chem. Soc.* 117:11085–11097.

Jentzen, W., X.-Z. Song, and J. A. Shelnutt. 1997. Structural characterization of synthetic and protein-bound porphyrins in terms of the lowest-frequency normal coordinates of the macrocycle. *J. Phys. Chem. B.* 101:1684–1699.

Jentzen, W., I. Turowska-Tyrk, W. R. Scheidt, and J. A. Shelnutt. 1996. Planar solid-state and solution structures of (porphinato)nickel(II) as determined by x-ray diffraction and resonance Raman spectroscopy. *Inorg. Chem.* 35:3559–3567.

Kratky, C., R. Waditschatka, C. Angst, J. Johansen, J. C. Plaquevent, J. Schreiber, and A. Eschenmoser. 1982. Die Sattelkonformation der hydroporphinoiden Nickel(II)-Komplexe: Struktur, Ursprung und stereochemische Konsquenzen. *Helv. Chim. Acta.* 68:1312–1337.

Kubitscheck, U., W. Dreybrodt, and R. Schweitzer-Stenner. 1986. Detection of heme distortions in ferri- and ferrocytochrome *c* by resonance Raman scattering. *Spectrosc. Lett.* 19:681–690.

Kunishima, N., K. Fukuyama, H. Matsubara, H. Hatanaka, Y. Shibano, and T. Amachi. 1994. Crystal structure of the fungal peroxidase from *Arthromyces ramosus* at 1.9-Å resolution: structural comparisons with the lignin and cytochrome *c* peroxidases. *J. Mol. Biol.* 235:331–344.

Lesk, A. M., and C. H. Chotia. 1986a. The response of protein structures to amino-acid-sequence changes. *Philos. Trans. R. Soc. Lond. A.* 317: 345–356.

Lesk, A. M., and C. H. Chotia. 1986b. Alignment of the amino-acid sequences of distantly related proteins using variable gap penalties. *Protein Eng.* 1:77–78.

Li, H., and T. L. Poulos. 1995. Modeling protein substrate interactions in the heme domain of cytochrome P450(Bm-3). *Acta Crystallogr. D.* 51:21–32.

Louie, G. V., and G. D. Brayer. 1990. High-resolution refinement of yeast iso-1 cytochrome *c* and comparisons with other eukaryotic cytochromes *c*. *J. Mol. Biol.* 214:527–555.

Luzzati, P. V. 1952. Traitement statistique des erreurs dans la determination des structures cristallines. *Acta Crystallogr.* 5:802–810.

Matias, P. M., C. Frazao, J. Morais, M. Coll, M. A. Carrondo. 1993. Structure analysis of cytochrome c_3 from *Desulfovibrio vulgaris* Hildenborough at 1.9-Å resolution. *J. Mol. Biol.* 234:680–699.

Matias, P. M., J. Morais, R. Coelho, M. A. Carrondo, K. Wilson, Z. Dauter, and L. Sieker. 1996. Cytochrome c_3 from *Desulfovibrio gigas*: crystal structure at 1.8-Å resolution and evidence for a specific calcium-binding site. *Protein Sci.* 5:1342–1354.

Matsuura, Y., T. Takano, and R. E. Dickerson. 1982. Structure of cytochrome c_{551} from *Pseudomonas aeruginosa* refined at 1.6 Å resolution and comparison of the two redox forms. *J. Mol. Biol.* 156:389–409.

Medforth, C. J., M. O. Senge, K. M. Smith, L. D. Sparks, and J. A. Shelnutt. 1992. Nonplanar distortion modes for highly substituted porphyrins. *J. Am. Chem. Soc.* 114:9859–9869.

Meyer, E. F. 1972. The crystal and molecular structure of nickel(II)octaethylporphyrin. *Acta Crystallogr. B.* 28:2162–2167.

Morais, J., P. N. Palma, C. Frazao, J. Caldeira, I. Moura, J. LeGall, J. J. G. Moura, and M. A. Carrondo. 1995. Structure of the tetraheme cytochrome from Desulfovibrio desulfuricans ATCC-27774: x-ray diffraction and electron paramagnetic resonance studies. *Biochemistry.* 34: 12830–12841.

Morimoto, Y., T. Tani, H. Okumura, Y. Higuchi, and N. Yasuoka. 1991. Effects of amino-acid substitution on three-dimensional structure: an x-ray analysis of cytochrome c_3 from *Desulfovibrio vulgaris* Hildenborough. *J. Biochem. (Tokyo).* 110:532–540.

Ochi, H., Y. Hata, N. Tanaka, M. Kakudo, T. Sakurai, S. Aihara, and Y. Morita. 1983. Structure of rice ferricytochrome at 2.0 Å resolution. *J. Mol. Biol.* 166:407–418.

Phillips, S. E. V., and B. P. Schoenborn. 1981. Neutron diffraction reveals oxygen-histidine hydrogen bond in oxymyoglobin. *Nature.* 292:81–82.

Poulos, T. L., B. C. Finzel, and A. J. Howard. 1986. Crystal-structure of substrate-free *Pseudomonas putida* cytochrome P450. *Biochemistry.* 25: 5314–5322.

Sayle, R., and E. J. Milner-White. 1995. RASMOL: biomolecular graphics for all. *Trends Biochem. Sci.* 20:374–376.

Scheidt, W. R., and M. Gouterman. 1983. Ligands, spin state, and geometry in hemes and related metalloporphyrins. *In* Iron Porphyrins, Part 1. A. B. P. Lever and H. B. Gray, editors. Addison-Wesley, London. 89–139.

Scheidt, W. R., and C. A. Reed. 1981. Spin-state/stereochemical relationships in iron porphyrins: implications for the hemoproteins. *Chem. Rev.* 81:543–555.

Schomaker, V., J. Waser, R. E. Marsh, and G. Bergman. 1959. To fit a plane or a line to a set of points by least squares. *Acta Crystallogr.* 12:600–604.

Shelnutt, J. A., S. A. Majumder, L. D. Sparks, J. D. Hobbs, C. J. Medforth, M. O. Senge, K. M. Smith, M. Miura, and J. M. E. Quirke. 1992. Resonance Raman spectroscopy of non-planar nickel porphyrins. *J. Raman Spectrosc.* 23:523–529.

Shelnutt, J. A, C. J. Medforth, M. D. Berber, K. M. Barkigia, and K. M. Smith. 1991. Relationships between structural parameters and Raman frequencies for some planar and nonplanar nickel(II) porphyrins. *J. Am. Chem. Soc.* 113:4077–4087.

Shelnutt, J. A., X.-Z. Song, J.-G. Ma, S.-L. Jia, W. Jentzen, and C. J. Medforth. 1997. Nonplanar porphyrins and their significance in proteins. *Chem. Soc. Rev.* (in press).

Song, X.-Z., W. Jentzen, S.-L. Jia, L. Jaquinod, D. J. Nurco, C. J. Medforth, K. M. Smith, and J. A. Shelnutt. 1996. Representation of nonplanar structures of nickel(II) 5,15-disubstituted porphyrins in terms of displacements along the lowest-frequency normal coordinates of the macrocycle. *J. Am. Chem. Soc.* 118:12975–12988.

Stampf, D. R., C. E. Felder, and J. L. Sussman 1995. PDBBROWSE: a graphics interface to the Brookhaven Protein Data Bank. *Nature.* 374: 572–574.

Sundaramoorthy, M., K. Kishi, M. H. Gold, and T. L. Poulos. 1994. Preliminary crystallographic analysis of manganese peroxidase from *Phanerochaete chrysosporium*. *J. Mol. Biol.* 238:845–848.

Sweet, R. M. 1986. Evolutionary similarity among peptide segments is a basis for prediction of protein folding. *Biopolymers.* 25:1565–1577.

Takano, T. 1984. Refinement of myoglobin and cytochrome *c*. *In* Methods and Applications in Crystallographic Computing. S. R. Hall and T. Ashida, editors. Oxford University Press, Oxford. 262–272.

Takano, T., and R. E. Dickerson. 1980. Redox conformation changes in refined tuna cytochrome *c*. *Proc. Natl. Acad. Sci. USA.* 77:6371–6375.

Waditschatka, R., C. Kratky, B. Jaun, J. Heinzer, and A. Eschenmoser. 1985. Chemistry of pyrrocorphins: structure of nickel(II) ccccc-octaethyl-pyrrocorphinate in the solid-state and in solution: observation of the inversion barrier between enantiomorphically ruffled conformers. *J. Chem. Soc. Chem. Commun.* 1604–1607.

Yang, F., and G. N. Phillips. 1996. Crystal structures of Co-myoglobins, deoxymyoglobins and metmyoglobins at various pH values. *J. Mol. Biol.* 256:762–774.